Design, Implementation, and Testing of Advanced Virtual Coordinate-Measuring Machines

Yang Hu, Qingping Yang, *Member, IEEE*, and Xizhi Sun

***Abstract*—Advanced virtual coordinate-measuring machines (CMMs) (AVCMMs) have recently been developed at Brunel University, which provide vivid graphical representation and powerful simulation of CMM operations, together with Monte-Carlo-based uncertainty evaluation. In an integrated virtual environment, the user can plan an inspection strategy for a given task, carry out virtual measurements, and evaluate the uncertainty associated with the measurement results, all without the need of using a physical machine. The obtained estimate of uncertainty can serve as a rapid feedback for the user to optimize the inspection plan in the AVCMM before actual measurements or as an evaluation of the measurement results performed. This paper details the methodology, design, and implementation of the AVCMM system, including CMM modeling, probe contact and collision detection, error modeling and simulation, and uncertainty evaluation. This paper further reports experimental results for the testing of the AVCMM.**

***Index Terms*—Advanced virtual coordinate-measuring machine (AVCMM), finite-element modeling, Monte Carlo method, uncertainty evaluation.**

I. Introduction

EXISTING virtual coordinate-measuring machines (VCMMs) typically fall into two categories. The first kind is to simulate and represent the actual measurement process and, in particular, the path planning of a physical CMM. This kind of VCMMs normally utilizes 2-D/3-D graphical representation of the CMM and measurement process and provides operation interfaces similar to physical CMMs, to aid in offline path planning, remote monitoring, and operator training [1]–[5]. The second kind focuses on the evaluation of measurement uncertainty. This kind of VCMMs is essentially a mathematical model of CMMs and the measurement process. By taking into account various uncertainty sources and studying their propagations, these sources of uncertainties can be combined together to generate the expanded uncertainty and also give their distributions [6]–[10].

In recognition of the limitations of the existing VCMMs, particularly the absence of a comprehensive integrated system that covers functions related to multiple aspects of the CMM and allows different functions to seamlessly share data and interact with each other, the authors have proposed an advanced VCMM (AVCMM) system, which organically combines inspection simulation with uncertainty evaluation, thus improving the usability and efficiency of both [11], [12]. The proposed system uses universal model and data sets to support both aspects of functionalities, so that the system components can easily communicate with and provide feedback to each other. Users may carry out inspection planning in the AVCMM by operating a visual CMM model and then have the results of the planned tasks including the associated uncertainties quickly calculated and evaluated. Without involving a physical CMM in the inspection planning or evaluation of uncertainty, the AVCMM can greatly reduce the time and cost needed for such processes. Furthermore, as the package offers vivid 3-D visual representation of the virtual environment and supports operations similar to those of a physical CMM, it does not only allow the user to easily plan and optimize the inspection strategy but also provide a cost-effective risk-free solution to the training of CMM operators.

The developed AVCMM system has a modular multitier architecture and incorporates a number of functional components covering CMM and work piece modeling, error simulation, inspection simulation, feature calculation, uncertainty evaluation, and 3-D representation. This design offers compatibility with various types of CMMs, extensibility of functions, and reusability of important components. A new engine for detecting contact/collision has been developed and utilized, which is suitable for the virtual environment of simulated CMM inspections. A novel approach has been established to calculate errors required for the error simulation, where the data are obtained from finite-element analysis (FEA) simulations in addition to an experimental method. The Monte Carlo method has been adopted for uncertainty evaluation and has been implemented with multiple options available to meet different requirements.

While the general approach and performance of the AVCMM system have been described in [12], this paper presents additional implementation details about the CMM modeling and probe error modeling, which are the key modules of the AVCMM, together with more experimental results and detailed discussions of the system testing procedure.

II. Design and Implementation

The AVCMM has an open architecture and a configurable platform that can simulate the behaviors of different types of CMMs and can predict or estimate measurement uncertainties

Manuscript received June 20, 2011; revised August 21, 2011; accepted September 7, 2011. Date of publication December 9, 2011; date of current version April 6, 2012. The Associate Editor coordinating the review process for this paper was Shervin Shirmohammadi.

Y. Hu was with the School of Engineering and Design, Brunel University, UB8 3PH Uxbridge, U.K. He is now with Sichuan Huaneng Fujiang Hydropower Company, Ltd., China Huaneng Group, Chengdu 610041, China (e-mail: chris.yang.hu@gmail.com).

Q. Yang and X. Sun are with the School of Engineering and Design, Brunel University, UB8 3PH Uxbridge, U.K. (e-mail: ping.yang@brunel.ac.uk).

Color versions of one or more of the figures in this paper are available online at http://ieeexplore.ieee.org.

Digital Object Identifier 10.1109/TIM.2011.2175828

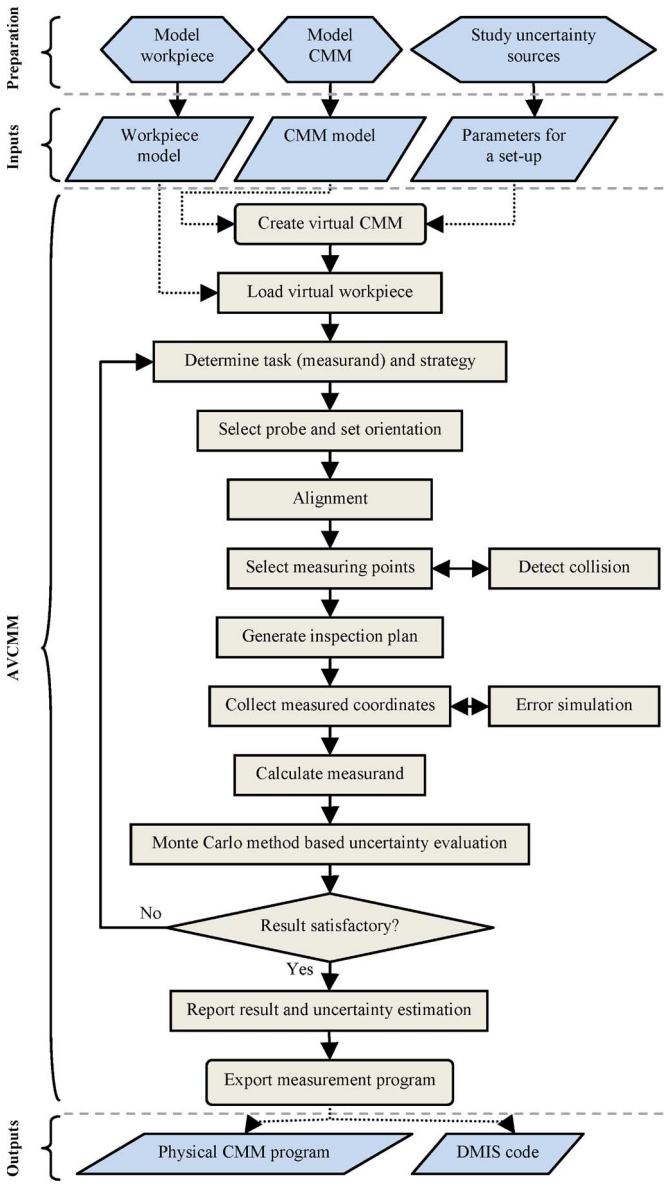

Fig. 1. Work flow of the AVCMM.

for user-defined inspection plans, hence allowing the user to improve or evaluate the inspection strategy. It has a work flow similar to the general procedure of manual CMM measurement but with substantial additions. Fig. 1 shows the general work flow of the AVCMM.

Due to the complexity of the AVCMM and the consideration for extensibility and scalability, a multitier architecture is adopted for its development. Fig. 2 shows the layout of the N-tier architecture design of the AVCMM. It consists of three major layers, namely, a model layer, a logic layer, and an interface layer. The logic layer itself is a three-tier structure, so the whole system becomes a five-tier architecture.

In the model layer, there are two modules that organize all the Virtual Reality Modeling Language (VRML) models used in the system. They are responsible for retrieving any specific model when required.

The logic layer itself has three sublayers. At the bottom, a VRML parser is responsible for extracting the geometrical information from the loaded VRML files and transforming the information into geometric equations or formulas. These formulas will later be utilized to enable the collision detection in virtual inspection. The middle sublayer of the logic layer is the core of the AVCMM system. In this sublayer, the virtual CMM module is located, and in turn, it has several submodules that handle the essential tasks respectively, i.e., loading the virtual work piece, configuring the virtual probe, controlling the movement of the virtual CMM, simulating various kinds of errors, detecting contact and collision, recording probed points, recording the inspection path, and calculating parameters for desired feature. Another important module also located in this sublayer is the uncertainty evaluation module, which carries out Monte Carlo simulation of the recorded inspection plan and calculates the uncertainty from the statistical analysis of the simulation results. In the top sublayer of the logic layer, a mediator module acts as a middleman that coordinates the communication and cooperation between the virtual CMM module and the uncertainty evaluation module. It also abstracts and exposes the interface of the whole logic layer to the higher interface layer.

In the interface layer, the graphical user interface is presented, which consists of a virtual console that mimics the CMM control console, a 3-D visual representation window that displays the virtual environment, and a user interface for controlling the uncertainty evaluation. The support for various kinds of input devices is also implemented here. Apart from the user interface, other interfaces are provided for further extension of the system, for example, a Dimensional Measuring Interface Standard (DMIS) converter that outputs the inspection path as a standard DMIS code so that the inspection program can be exported to other DMIS-savvy systems. Furthermore, the application programming interface of the whole AVCMM system is abstracted and defined so that further development or integration can be made upon the system.

A. CMM Modeling

VRML is used to model both CMMs and work pieces in the AVCMM system. In addition to simple geometrical modeling, the methodology of transforming CMM kinematical models into VRML models has been established, so that CMMs with different configurations can be virtualized with corresponding VRML models that represent different kinematical characteristics, as shown in Figs. 3 and 4. When modeling these five common types of CMMs, the following constraints were taken into consideration.

1) A machine coordinate system should be defined, and its relationship to the native VRML coordinate system should be established. This can be archived by constructing a transformation matrix T and a translation vector L so that

$$\begin{bmatrix} X_{\mathrm{CMM}} \\ Y_{\mathrm{CMM}} \\ Z_{\mathrm{CMM}} \end{bmatrix} = T \begin{bmatrix} X_{\mathrm{VRML}} \\ Y_{\mathrm{VRML}} \\ Z_{\mathrm{VRML}} \end{bmatrix} + L \tag{1}$$

where subscript "CMM" denotes the coordinates in the established machine coordinate system and subscript "VRML" denotes the coordinates in the VRML native

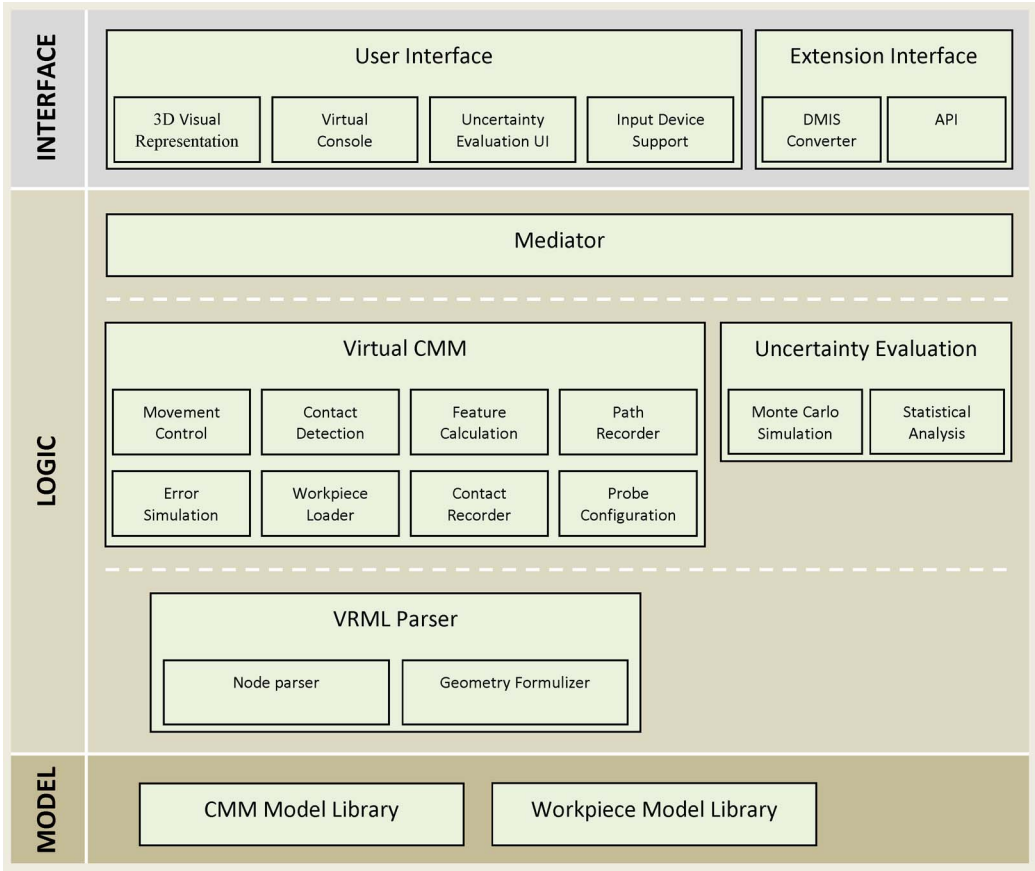

Fig. 2. N-tier architecture of the AVCMM.

coordinate system. Matrix T describes the rotation between the two coordinate systems, and vector L is the distance between the two origins.

2) The travel range of each axis in the VRML model should comply with the measurement volume of the CMM being modeled. This is to ensure that the location-related uncertainty can be properly taken into consideration later in the error simulation.
3) The positions of the three axes X_{axis}, Y_{axis}, and Z_{axis} in the machine coordinate system should correspond to the actual coordinates of the CMM (X_a, Y_a, Z_a) with a simple relationship

$$\begin{bmatrix} X_a \\ Y_a \\ Z_a \end{bmatrix} = \text{diag}\left(\begin{bmatrix} X_{\text{axis}}(X) & X_{\text{axis}}(Y) & X_{\text{axis}}(Z) \\ Y_{\text{axis}}(X) & Y_{\text{axis}}(Y) & Y_{\text{axis}}(Z) \\ Z_{\text{axis}}(X) & Z_{\text{axis}}(Y) & Z_{\text{axis}}(Z) \end{bmatrix} \right) = \begin{bmatrix} X_{\text{axis}}(X) \\ Y_{\text{axis}}(Y) \\ Z_{\text{axis}}(Z) \end{bmatrix} \quad (2)$$

where diag means the diagonal of a matrix. In this way, the control of the CMM movement and the retrieval of current coordinates are interfaced between the VRML world and other modules with a single vector (X_a, Y_a, Z_a), which can be easily transformed into the VRML native coordinate system using (1).

4) The axes X, Y, and Z of the CMM model should be able to travel individually and simultaneously. The relationships between each axis must be considered in order to construct an efficient model in terms of using as few parameters as possible to decide and describe the state of the machine. Fig. 5 shows a bad example of VRML model design that uses a flat layout and thus requires the three axes to be controlled by three vectors, one for each axis, containing duplicated information. In VRML, an object is composed of a set of basic shapes. Each shape is embedded in a transform node that has a translation property controlling the position of the node and a rotation property controlling the orientation of the node. Transform nodes can be grouped together, can be children of other transform nodes, and can have their own children transform nodes. The translation and rotation properties are all relative to that of the parent transform node. A better design of the modeling of CMM, as shown in Figs. 3 and 4, should make use of the hierarchical structure of VRML nodes and implement relative movement using the relative translation between parent and children nodes.

B. Contact and Collision Detection

Since VRML has no native object-to-object collision detecting mechanism, a contact and collision detection engine is needed to enable the point sampling and collision detection in the virtual environment. To avoid the inconvenience of deploying third-party packages or the limitation of using some particular browsers, a new contact and collision detection engine was

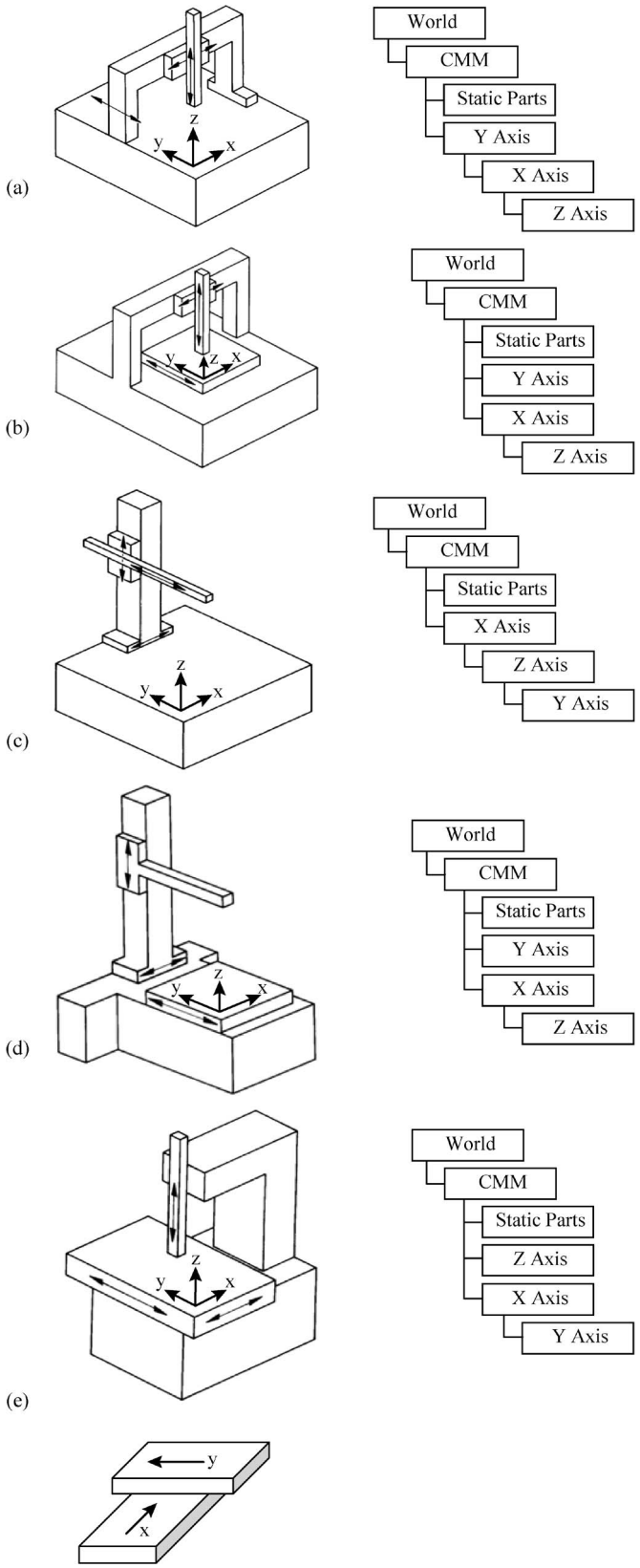

Fig. 3. VRML model designs for five common CMM configurations. (a) Moving-bridge CMM. (b) Fixed-bridge CMM. (c) Moving-horizontal-arm CMM. (d) Fixed-horizontal-arm CMM. (e) Column CMM.

designed and developed for the AVCMM system. To achieve universal compatibility and easy deployment, the browser is released from the responsibility of collision detection, and the function is implemented inside the AVCMM. A substep routine is used in this engine to resolve the conflict between detection accuracy and speed.

When measuring a work piece in the AVCMM system, let v_m be the measurement speed of the probe and N_m be the number of movements (steps) that the system can perform per second; then, the length of each step $\delta_m = v_m/N_m$. Restricted by the time and cost of the algorithms at each step, the current system can perform roughly tens to hundreds of steps per second. If v_m is set to be close to a real measurement speed, which is usually at the level of several millimeters per second, then the step length δ_m is much longer than a typical CMM's resolution δ_r, which means that the resulted coordinates are not accurate enough to represent a sample point. To overcome this problem and achieve the same level of resolution as the modeled CMM, an additional routine is used so that, each time when a contact is detected, the step δ_m between the contacted position and the previous position is divided into N_s number of substeps, so that the length of each substep $\delta_s = \delta_r = \delta_m/N_m$. Then, as shown in Fig. 6, the tip is retested for contact with the work piece along the path of N_s substeps to find the point of contact which has the same resolution as the modeled CMM. This routine is performed without updating the 3-D graphical view at each substep, so the serial of testing can be finished very rapidly.

C. Error Modeling and Simulation

This research has focused on the simulation of the CMM geometric errors and probe errors as their complexity alone requires nontrivial investigations. Error map is an effective way to represent and utilize such errors. Probe errors were evaluated by measuring a reference sphere at certain intervals along latitude and longitude directions [13], although other techniques may also be used [14]. The errors (deviations of the distances between the measured points and the sphere center from the sphere radius) are stored in a 2-D matrix which can be indexed by the latitude and longitude of sampling direction. Furthermore, since the errors of a touch-trigger probe are affected by the stylus length and the probe tilt angle (A), a probe error map was constructed for each probe configuration ($A = 0°, 45°,$ and $90°$; $L = 30, 60,$ and 80 mm), with some examples shown in Fig. 7.

When the probe is tilted and rotated, because the error map is defined with respect to the probe coordinate system, the probing direction in the machine coordinate system must be transformed to the probe coordinate system. This can be done by the operation of a transformation matrix T_p. Let A be the tilting angle and B be the rolling angle of the probe; the relationship between the machine coordinate system (x, y, z) and the probe coordinate system (x', y', z') can be expressed as

$$\begin{bmatrix} x' \\ y' \\ z' \end{bmatrix} = T_p \begin{bmatrix} x \\ y \\ z \end{bmatrix} \tag{3}$$

where

$$T_p = \begin{bmatrix} \cos A \cos B & -\sin B & -\sin A \cos B \\ \cos A \sin B & \cos B & -\sin A \sin B \\ \sin A & 0 & \cos A \end{bmatrix}. \tag{4}$$

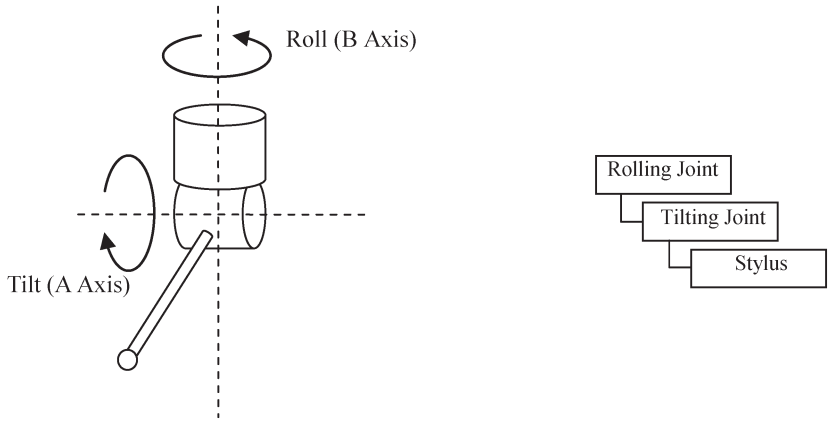

Fig. 4. VRML model designs for a probe.

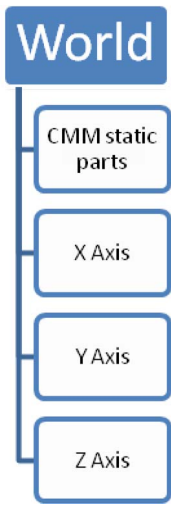

Fig. 5. Example of a bad VRML model design.

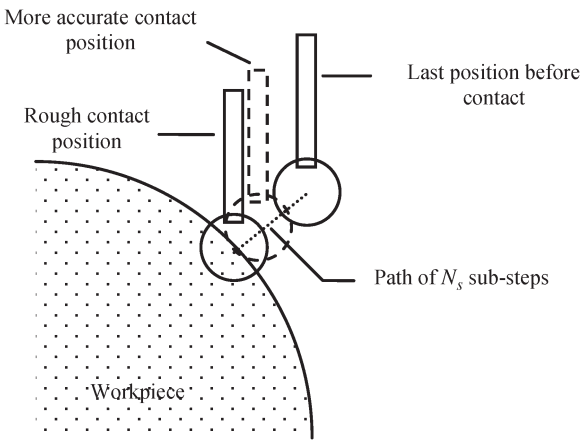

Fig. 6. Determination of more accurate contact position.

When a point is sampled in the AVCMM, the contact position $P_C = [X_C, Y_C, Z_C]^{\mathrm{T}}$ and the last position before contact $P_L = [X_L, Y_L, Z_L]^{\mathrm{T}}$ are used to decide the probing direction. The free vector v pointing from P_L to P_C is given by

$$v = \overrightarrow{P_L P_C} = \begin{bmatrix} \Delta x \\ \Delta y \\ \Delta z \end{bmatrix} = \begin{bmatrix} X_C - X_L \\ Y_C - Y_L \\ Z_C - Z_L \end{bmatrix}. \tag{5}$$

A unit vector $\hat{v} = [M_x, M_y, M_z]^{\mathrm{T}}$ representing the probing direction can then be obtained by

$$\hat{v} = \frac{v}{\|v\|} = \frac{v}{\sqrt{\Delta x^2 + \Delta y^2 + \Delta z^2}}. \tag{6}$$

Since the direction $\hat{v}$ is defined in the machine coordinate system, it must be transferred to the probe coordinate system by

$$\hat{v}' = \begin{bmatrix} M_x' \\ M_y' \\ M_z' \end{bmatrix} = T_p \hat{v} = T_p \begin{bmatrix} M_x \\ M_y \\ M_z \end{bmatrix} \tag{7}$$

where $\hat{v}'$ is the unit vector representing the probing direction in the probe coordinate system and T_p is the transformation matrix defined in (4). The latitude θ and longitude ϕ of the probing direction can be calculated from $\hat{v}'$

$$\theta = \sin^{-1}\left(\frac{M_z'}{\|\hat{v}'\|}\right) = \sin^{-1}\left(M_z'\right) \tag{8}$$

$$\phi = \tan^{-1}\left(\frac{M_y'}{M_x'}\right). \tag{9}$$

The obtained angles (θ and ϕ) are used to retrieve the measured probe error from the closest interval in the error map. Before it can be added to the measurement result, the retrieved probe error $E_p(\theta, \phi)$, which is a deviation along the probing direction in the machine coordinate system, should first be resolved into three components along the three axes of the machine coordinate system according to the probing direction $\hat{v}$

$$\begin{bmatrix} \varepsilon_{p,x} \\ \varepsilon_{p,y} \\ \varepsilon_{p,z} \end{bmatrix} = E_p(\theta, \phi)\hat{v} \tag{10}$$

where $\varepsilon_{p,x}$, $\varepsilon_{p,y}$, and $\varepsilon_{p,z}$ are the resolved probe error components.

For the CMM geometric errors, in addition to the well-established mathematical models for volumetric error calculation [7], finite-element method is also implemented to acquire the geometric errors. The FEA of the CMM static structure is performed using ANSYS software. The structure of the CMM is modeled with the following assumptions: 1) rigid connection between components; 2) the geometric errors being caused

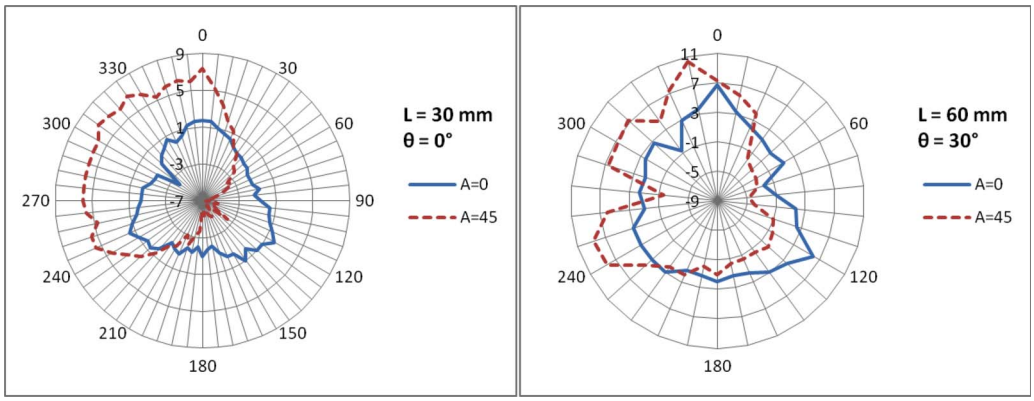

Fig. 7. Example probe error maps.

TABLE I
MATERIAL PROPERTIES USED IN THE FEA

Material	Elastic Modulus (GPa)	Poisson's Ratio	Density (g/cm^3)
Aluminium Alloy	79	0.33	2.7
Steel	210	0.3	7.8
Granite	40	0.3	2.6

by the structural deformation due to gravitational force; and 3) simplification of certain geometrical shapes (e.g., fillets and chamfers). The material properties used for the model are given in Table I. The bottom area of the base in the CMM model is constrained completely (all six degrees of freedom). Since the CMM loading depends upon the location of the probe, simulation has to be performed at multiple locations in the measuring volume at certain interval. At each location, a CMM model is created using the ANSYS Parametric Design Language. Fig. 8(a) shows the result of an FEA carried out at one location as an example. The displacement of the probe head relative to the measuring table should largely represent the combined geometric error at that location. The FEA model is then modified with the probe head moved to different locations, and the simulation is repeated until the CMM measuring volume has been adequately sampled. The results generated hence define a geometric error map, indexed by the axis positions, as shown in Fig. 8(b).

It should be noted that the error mapping for both machine geometric errors and probe errors mostly addresses only the systematic errors. The random errors may be estimated by repeatedly measuring a set of points in the measuring volume. For the AVCMM prototype, eight points on a ring gauge have been measured in four setups at different locations and orientations in the measuring volume, and five points on a reference sphere have been measured at one location, amounting to 37 points on the two artifacts. For each point, the measurement has been repeated 30 times; therefore, a total number of 1110 measurements have been made for all 37 points. The random errors were determined based upon the variations of the individual measurements from the average results of measurement at all these points, as shown in Fig. 9. Based on a large number of measurements, the probability distribution function can be obtained, and the repeatability can be determined, which is then used to construct the random errors in the AVCMM.

D. Uncertainty Evaluation

The uncertainty evaluation in the AVCMM was implemented using the Monte Carlo method, and it complies with the requirements of The Guide to the Expression of Uncertainty in Measurement (GUM) Supplement 1 [15]. It was designed to work in two modes: 1) *a priori* mode and 2) adaptive mode. In *a priori* mode, the number of Monte Carlo trials is specified by the user. In the adaptive mode, the simulation performs an increasing number of trials until the results have stabilized in a statistical sense, i.e., until twice the standard deviations associated with the numerical results are less than the numerical tolerance associated with the standard uncertainty of the measurement results.

To allow either visual demonstration or fast computation, the uncertainty evaluation module has been implemented to work in two ways. The first one is to automatically repeat the measurement program recorded in manual or learning mode to obtain the sample results. When repeating, the virtual machine would go through every step recorded or programmed. The user may choose to switch on/off the visualization option, which determines whether the uncertainty evaluation module updates the display of VRML world in real time. Although this "repetition" way of simulation is somehow time consuming, it retains all the details in the inspection process, and it also allows for additional error contributors to be included in the process. In the first prototype, only geometric errors and probe errors, together with the random error components, were considered, and in a given setup, only contact positions and probing directions are required to simulate these errors. Therefore, a faster simulation method is also implemented. In the manual mode, the true value of each contact point, i.e., the coordinates before errors are added, is recorded, together with the probing direction at each point. Later in the simulation module, these coordinates and directions are repeatedly used to look up the error maps to generate sets of points with simulated errors. These generated points are then sent to the feature calculation module to obtain simulated measurement results. Since the inspection progress is not repeated, this method allows the simulation to run much faster.

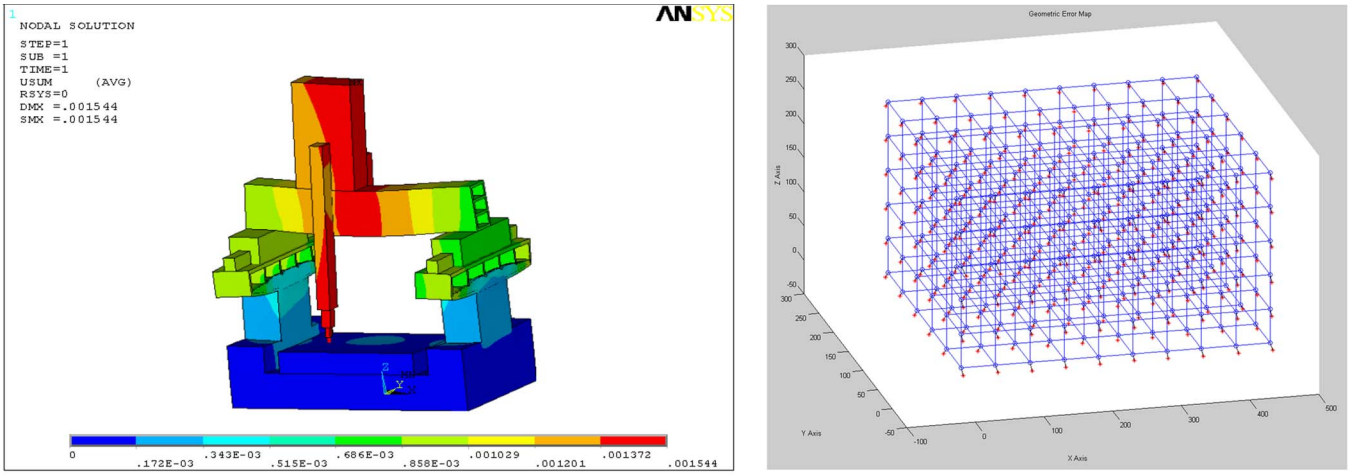

(a) (b)

Fig. 8. (a) FEA result for the following location: $X = 101$ mm, $Y = 151$ mm, and $Z = 51$ mm. (b) Geometric error map.

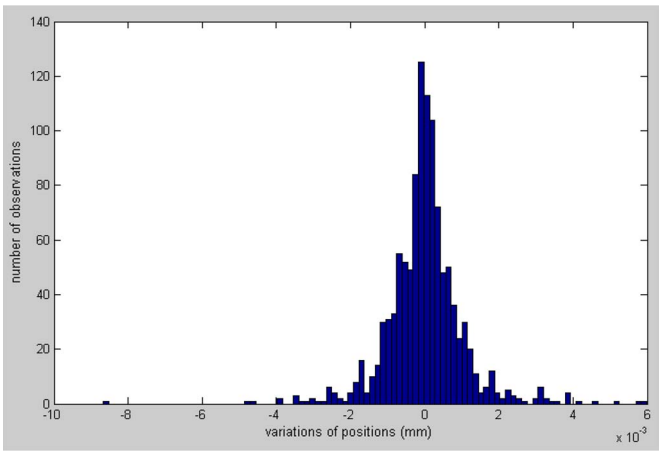

Fig. 9. Distribution of the random experimental errors.

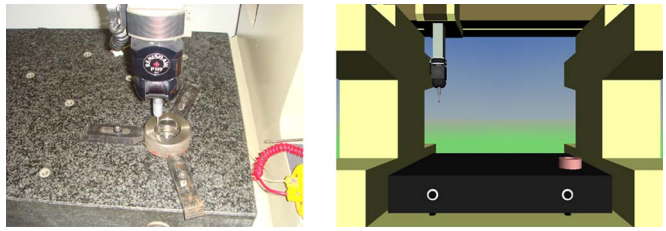

Fig. 10. Example setup.

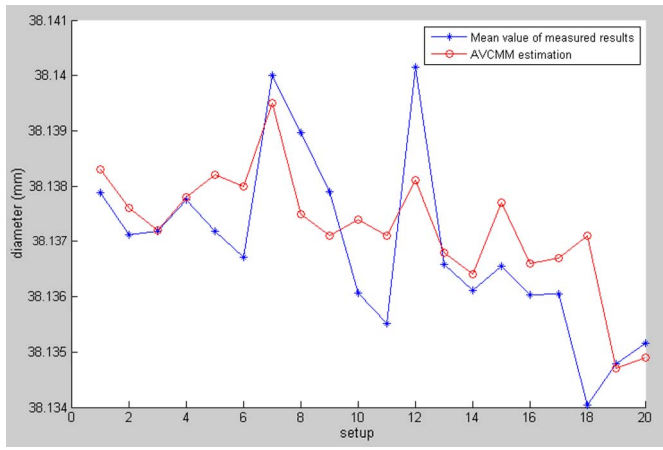

Fig. 11. Measurement results versus AVCMM estimation.

III. Experimental Results and System Testing

Following the implementation of an AVCMM prototype, its general performance and the uncertainty evaluation, in particular, need to be carefully tested. The general approach involves carrying out a number of measurements of a calibrated artifact on a physical CMM and statistically comparing the observed results with the results predicted by the AVCMM, as this is the most direct method of examining the validity of an uncertainty statement produced by computer simulation [16]. The experiments were performed in a temperature-controlled laboratory, and temperature was recorded in all measurements to correct the results to 20.0 °C. The inspections were performed at 20 setups with different locations and orientations. Fig. 10 shows an example of a setup in both physical and virtual inspections.

For each setup, the mean value of the ring gauge bore diameter was calculated from 30 measurements, and at the same time, the AVCMM produced an estimated result for that setup. Fig. 11 shows a comparison of these two sets of results, which clearly indicate that the results predicted by the AVCMM are in good agreement with the measured results in terms of their distribution, overall trend, and pattern. The predicted results are somewhat slightly "flatter" than the measured results, where the standard deviation of the former is 1.1 μm and that of the latter is 1.6 μm. This difference may be attributed to the fact that the actual measurements were affected by additional uncertainty sources that are not included in this AVCMM prototype.

For detailed analysis, the 30 measured values of the bore diameter at each setup were compared to the coverage interval obtained from the corresponding simulation in the AVCMM. Fig. 12 plots both measured values and predicted coverage interval for 4 of the 20 setups as examples. The calibrated value of the bore diameter is also marked for reference. After analysis of all 20 setups, it can be seen that, for most setups, the predicted coverage interval encompasses all or majority of the measured values, and for almost all setups, at least some of the measured values are covered by the predicted coverage

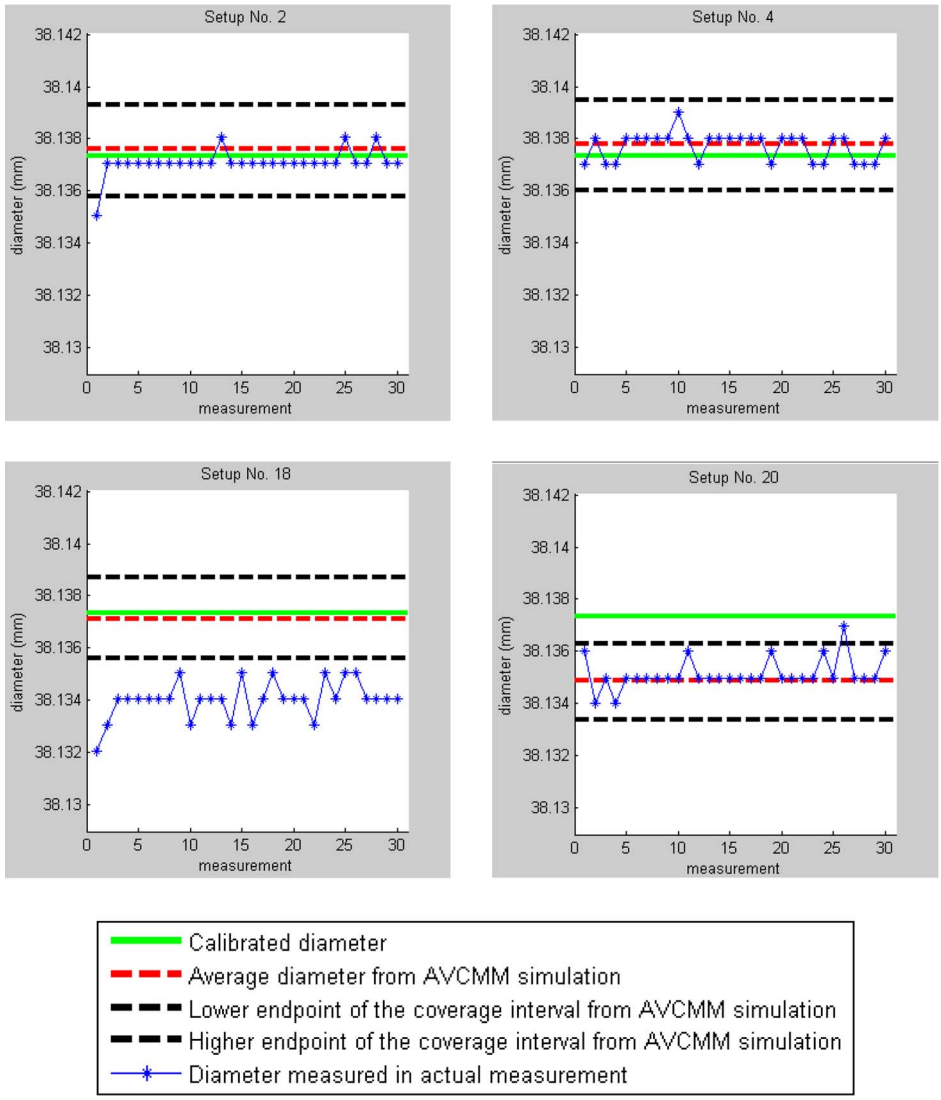

Fig. 12. Measurement results versus coverage interval predicted by the AVCMM.

interval, with the only exception of setup 18. At setup 18, the measured values clearly deviate from the predicted result and coverage interval, and this deviation may be due to a number of possible reasons including the following: 1) form deviation of the ring gauge; 2) difference between actual and virtual probing directions; 3) effects of other unconsidered uncertainty contributors; and 4) other unnoticed errors introduced during measurements.

In compliance with the recommendation of ISO 15530-4:2008 regarding the methods of testing uncertainty-evaluating software [17], the measurement results were tested against the expanded uncertainties evaluated by the AVCMM after compensation of systematic effects. First, the 20 mean values of the measurement results at 20 setups were tested against their associated task-specific expanded uncertainties determined by the AVCMM, to find out the proportion of the cases where the plausibility criterion was satisfied. The criterion is that a statement of uncertainty is plausible if

$$\frac{|\overline{y} - y_{\text{cal}}|}{\sqrt{U_{\text{cal}}^2 + U^2}} \leq 1 \tag{11}$$

where $\overline{y}$ is the mean value of the results of 30 repeated measurements at each setup, $y_{\text{cal}} = 38.13735$ mm is the calibrated value of the bore diameter, $U_{\text{cal}} = 0.00009$ mm is the expanded uncertainty of the calibrated diameter of the bore, with coverage factor $k = 2$, and U is the task-specific expanded uncertainty determined by the AVCMM for each setup, also with coverage factor $k = 2$.

Based upon the experimental results, we found that the plausibility criterion was satisfied for 18 out of the 20 setups, or 90% of the time, which is very close to the ideal proportion 95%.

Furthermore, each individual measurement within each of the 20 setups was tested against the coverage of the related uncertainty ranges. The plausibility criterion used is slightly different from (11)

$$\frac{|y - y_{\text{cal}}|}{\sqrt{U_{\text{cal}}^2 + U^2}} \leq 1 \tag{12}$$

where y is the result of each individual measurement and y_{cal}, U_{cal}, and U remain unchanged.

The overall proportion of plausible cases was found to be 81%. With some adjustment applied, i.e., including "edge points" as plausible cases and rejecting obvious outliers, the overall proportion reached 95%.

IV. Conclusion

This paper has reported the details of the design, implementation, and testing of a novel AVCMM system, in which, for the first time, the inspection planning and uncertainty evaluation of CMM measurements have been integrated. The system employs a novel method of transforming CMM kinematical models into VRML models, together with the contact and collision detection engine developed. Both CMM geometric (volumetric) errors and probe errors have been incorporated in the error simulator of the AVCMM, with the error data obtained from FEA and actual measurements. A Monte-Carlo-based uncertainty evaluation module has also been implemented with multiple methods and options. The AVCMM system has been evaluated and compared with the physical testing on an individual CMM. The results have demonstrated that the developed AVCMM system can satisfy the plausibility criterion close to 95% of the time, with great potentials to improve the functionalities and overall performance of CMMs.

The AVCMM is extensible, which allows the future version of the AVCMM to integrate different types of errors (parametric and volumetric) and additional error sources (e.g., thermal errors and even software errors). Since the modeled errors are largely systematic, the AVCMM can be used for error compensation and optimization, greatly enhancing the CMM capability.

An interface is under development to allow communication between the AVCMM system and the physical CMM or its CMM software. The measurement program developed in the AVCMM may then be directly executed on the physical CMM, and the AVCMM can have access to the data measured by the physical CMM, together with the 3-D data processing and programming modules in the CMM software, providing risk-free online/offline inspection planning in a virtual environment and quick prediction or estimation of measurement uncertainty for planned or performed measurement tasks.

References

[1] Y. H. Chen, Y. Z. Wang, and Z. Y. Yang, "Towards a haptic virtual coordinate measuring machine," *Int. J. Mach. Tools Manuf.*, vol. 44, no. 10, pp. 1009–1017, Aug. 2004.

[2] Z. Yang and Y. Chen, "Inspection path generation in haptic virtual CMM," *Comput.-Aided Des. Appl.*, vol. 2, no. 1–4, pp. 273–282, 2005.

[3] Y. H. Chen, Z. Y. Yang, and Y. Z. Wang, "Haptic modelling for a virtual coordinate measuring machine," *Int. J. Prod. Res.*, vol. 43, no. 9, pp. 1861–1878, May 1, 2005.

[4] W. G. Lin, R. S. Che, and G. Chen, "A study of virtual inspection of virtual coordinate measuring machine," in *Proc. 4th ICEMI Conf.*, Harbin, China, 1999.

[5] X. L. Liu, S. Y. Ma, P. D. Wu, and Z. L. Chen, "An Internet-based measurement system for coordinate measurement machines," in *Proc. 2nd Int. Symp. Instrum. Sci. Technol.*, Jinan, China, 2002.

[6] B. van Dorp, H. Haitjema, F. Delbressine, R. Bergmans, and P. Schellekens, "Virtual CMM using Monte Carlo methods based on frequency content of the error signal," *Proc. SPIE—Int. Soc. Opt. Eng.*, vol. 4401, pp. 158–167, 2001.

[7] H. J. Pahk, M. Burdekin, and G. N. Peggs, "Development of virtual coordinate measuring machines incorporating probe errors," *Proc. Inst. Mech. Eng. B, J. Eng. Manuf.*, vol. 212, no. B7, pp. 533–548, Jul. 1998.

[8] F. Waldele and H. Schwenke, "Automated calculation of measurement uncertainties on CMMs—Towards industrial application," *Technisches Messen*, vol. 69, no. 12, pp. 550–557, Dec. 2002.

[9] W. Jakubiec and M. Starczak, "EMU—Friendly software for estimation of measurement uncertainty for CMM," in *Proc. 8th Int. Symp. Meas. Quality Control Production*, Erlangen, Germany, 2004, pp. 265–270.

[10] M. Trenk, M. Franke, and H. Schwenke, "The 'virtual CMM' a software tool for uncertainty evaluation—Practical application in an accredited calibration lab," in *Proc. ASPE Summer Top. Meeting Uncertainty Anal. Meas. Des. State College*, Pennsylvania, PA, 2004.

[11] Y. Hu, Q. Yang, and P. Wei, "Development of a novel virtual coordinate measuring machine," in *Proc. IEEE I2MTC*, Singapore, 2009, pp. 230–233.

[12] Y. Hu, Q. Yang, and X. Sun, "Development and experimental validation of an advanced virtual coordinate measuring machine," in *Proc. IEEE I2MTC*, Hangzhou, 2011, pp. 1392–1396.

[13] Q. Yang, C. Butler, and P. Baird, "Error compensation of touch trigger probes," *Measurement*, vol. 18, no. 1, pp. 47–57, May 1996.

[14] M. R. Salleh, Q. Yang, and B. E. Jones, "Evaluation of touch trigger probe measurement uncertainty using FEA," in *Proc. IEEE Instrum. Meas. Technol. Conf.*, Sorrento, Italy, 2006, pp. 833–836.

[15] *ISO Guide 98-3:2008/Suppl 1:2008 Propagation of Distributions Using a Monte Carlo Method*, International Organization for Standardization, Geneva, Switzerland, 2008.

[16] S. D. Phillips, B. R. Borchardt, A. Abackerli, C. M. Shakarji, D. S. Sawyer, P. Murray, B. Rasnick, K. Summerhays, J. M. Baldwin, and M. P. Henke, "The validation of CMM task specific measurement uncertainty software," in *Proc. ASPE Summer Tropical Meeting—Coordinate Measuring Machines*, Charlotte, NC, 2003, pp. 1–6.

[17] *ISO 15530-4:2008(E) Geometrical Product Specifications (GPS)—Coordinate Measuring Machines (CMM): Technique for Determining the Uncertainty of Measurement—Part 4: Evaluating Task-Specific Measurement Uncertainty Using Simulation*, International Organization for Standardization, Geneva, Switzerland, 2008.

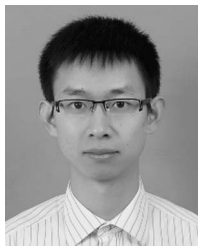

Yang Hu received the B.Eng. degree in computer science from the University of Electronic Science and Technology of China, Chengdu, China, in 2005 and the Ph.D. degree in virtual measurement systems from Brunel University, Uxbridge, U.K., in 2010.

He is currently with Sichuan Huaneng Fujiang Hydropower Company, Ltd., China Huaneng Group, Chengdu.

Qingping Yang (M'97) received the Ph.D. degree in high-precision dimensional metrology from Brunel University, Uxbridge, U.K., in 1992.

He is a Lecturer with Brunel University. His current research interests include advanced sensors, dimensional metrology, quality engineering, measurement science, and information and knowledge systems. He has published more than 70 papers in these areas.

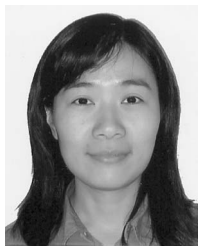

Xizhi Sun received the Ph.D. degree in precision manufacturing from Brunel University, Uxbridge, U.K., in 2009.

She is currently a Research Fellow with Brunel University. Her current research interests include the design and analysis of precision machine tools and the simulation of precision machining processes. She has published more than ten papers in these fields.